nature geoscience

LETTERS

PUBLISHED ONLINE: 14 AUGUST 2011 | DOI: 10.1038/NGEO1231

A record of the Southern Oscillation Index for the past 2,000 years from precipitation proxies

Hong Yan[1], Liguang Sun[1]*, Yuhong Wang[1,2], Wen Huang[3], Shican Qiu[4] and Chengyun Yang[4]

The El Niño-Southern Oscillation (ENSO) is a coupled ocean–atmosphere climate phenomenon in the tropical Pacific Ocean. The interannual climate variations have been shown to modify both the Hadley and Walker meridional and zonal atmospheric circulations, with strong impacts on global climate[1–3]. Proxy-based reconstructions of the Southern Oscillation Index on a multi-decadal scale have shown that the strength and frequency of El Niño occurrences have varied over the past millennium[4–7]. Here we compile reconstructions of precipitation[8–15] from regions that experience substantial ENSO variability to extend the multidecadal-scale Southern Oscillation Index to include the past 2,000 years. We find that the Medieval Warm Period (~AD 800–1300) was characterized by a negative index, which indicates more El Niño-dominated conditions, whereas during the Little Ice Age (~AD 1400–1850) more La Niña-dominated conditions prevailed. The Southern Oscillation Index we derive is significantly correlated with reconstructions of solar irradiance and mean Northern Hemisphere temperature fluctuations.

The Southern Oscillation (SO) is principally a seesaw trend in atmospheric mass involving coherent exchanges of air between the eastern and western Pacific (Supplementary Fig. S1; ref. 2). The traditional Southern Oscillation index (SOI) is defined as the difference between the sea level pressure (SLP) of antiphase oscillatory behaviour at Tahiti, in the eastern Pacific, and Darwin, in the western Pacific[16]. Owing to the close link between SLP and local convection and precipitation, the rainfalls in the western Pacific and the eastern and mid Pacific are closely related to the SOI. For example, Trenberth and Caron (2000; ref. 2) examined the statistical relationship between the SOI and tropical Pacific precipitation and showed that the SOI is persistently and positively correlated with the precipitation over the Indo-Pacific warm pool and negatively correlated with the precipitation over the eastern and mid-tropical Pacific (Fig. 1, Areas in the equatorial Pacific where precipitation was significantly (above 95% confidence level) positively correlated with the SOI are marked in yellow and red (named positive area, or PA) and areas with significant negative correlation with the SOI are marked in green and blue (named negative area, or NA); ref. 2). The influence of the SO on equatorial Pacific precipitation can be explained by the variation of the Pacific Walker Circulation[3]. During an El Niño event, when the SOI is low, the difference of SLP between the eastern and western Pacific decreases. As a consequence, the Walker Circulation is weakened, and the ascending limb in the western Pacific switches to the mid-Pacific, leading to aridity in the western Pacific and humidity in the mid-Pacific. At the same time, the eastern tropical Pacific experiences a large increase, up to an order of magnitude, in precipitation owing to the weakened and transferred descending limb of the Walker Circulation.

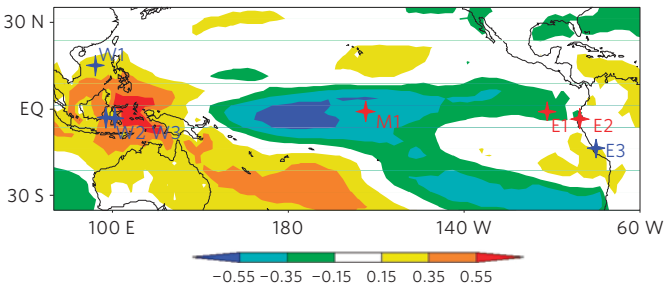

Figure 1 | Locations of hydrological records. Correlations of monthly anomalies of precipitation (NCEP reanalysis2) with the SOI from January 1979 to December 2010. Areas in equatorial Pacific with positive and significant correlation (above 95% confidence level) are marked in yellow and red, and areas with negative and significant correlation were marked in green and blue. Locations of the rainfall records in the equatorial Pacific (W1 (refs 8,11), W2 (refs 10,12), W3 (ref. 9), M1 (ref. 15), E1 (ref. 13), E2 (ref. 14) and E3 (ref. 22)) are also indicated. Locations that were drier/wetter during the Little Ice Age than during the Medieval Warm Period are marked in red/blue.

Based on such strong and persistent correlation between the SOI and precipitation, in this study, we proposed a novel and SOI-like index, SOI_{pr}, as the difference between normalized annual rainfalls in the PA of tropical western Pacific and the NA of the equatorial eastern and mid-Pacific ($SOI_{pr} = w_p Z_P - w_n Z_N$; where Z_P and Z_N are the normalized Z-scores of the precipitation in the PA and NA, respectively. w_p and w_n are the optimal weights of Z_P and Z_N and $w_p + w_n = 1$. See Methods and Supplementary Fig. S4 for details). To evaluate the feasibility of using SOI_{pr} as a SOI proxy, we calculated SOI_{pr} from AD 1951 to 1997 using the instrumental precipitation data from Galapagos of the eastern Pacific and Indonesia of the western Pacific (Supplementary Figs S3–S5). We observed a significant positive correlation between SOI_{pr} and the instrumental sea level pressure-based SOI (Supplementary Fig. S5, $r = 0.68$, $p < 0.0001$, $n_{eff} = 40.6$ (effective number of independent values; see Methods for details)), indicating that SOI_{pr} is indeed a good proxy for the SOI.

Recently, several rainfall reconstructions for the PA of the western Pacific[8–12] and the NA of the eastern[13,14] and mid Pacific[15] have been published (Fig. 1). The records from the PA (refs 8–12) and NA (refs 13–15) contained substantial multi-decadal variability, characterized by an anti-phase oscillatory behaviour over the last two millennia (Supplementary Fig. S6), and allowed us to reconstruct SOI_{pr} for the past two millennia. Considering these resolution and time span of these records (Supplementary Table S1 and Fig. S6), in this study we chose the

[1]Institute of Polar Environment, School of Earth and Space Science, University of Science and Technology of China, Hefei, Anhui 230026, China, [2]Institute of Oceanology, Chinese Academy of Sciences, Qingdao 266071, China, [3]Department of Dairy Science, University of Wisconsin, Madison, Wisconsin 53706, USA, [4]School of Earth and Space Science, University of Science and Technology of China, Hefei, Anhui 230026, China. *e-mail: slg@ustc.edu.cn.

precipitation records of Indonesia[10] and Galapagos[13] to calculate SOI_{pr} for the past two millennia. The Indonesian historic rainfalls (AD 25–1955) were derived from a salinity reconstruction based on planktonic-foraminifera $\delta^{18}O$ and the Mg/Ca ratio (ref. 10). The $\delta^{18}O$ of foraminiferal calcite ($\delta^{18}O_c$) reflects the combined effects of calcification temperature (T) and seawater oxygen isotope ($\delta^{18}O_w$); the latter varies as a function of salinity. The Mg/Ca ratio in the shells is primarily temperature dependent. By measuring both $\delta^{18}O_c$ and the Mg/Ca ratio on the same samples, the salinity component in the $\delta^{18}O$ signal can be extracted[10]. The salinity component indicates the precipitation-caused freshening trend of the surface water in the Indo-Pacific Warm Pool and is thus an indicator of precipitation. The rainfall history of the Galapagos (7241 BC–AD 2004) is derived from a lake level reconstruction which is based on the grain size data from the Lago El Junco sediment core[13]. As suggested in the hydro-climatic model simulations, El Junco lake sediment grain size responds sensitively to the precipitation changes associated with the Pacific Walker Circulation (PWC) and El Niño events, increasing during wet El Niño events (weak PWC) and decreasing during the intervening dry periods[13].

The reconstructed precipitation in the Indo-Pacific has an average resolution of 10 years, and that in Galapagos of 11 years. We adjusted the two records to one year resolution using linear interpolation, normalized them, and calculated SOI_{pr} for the time period from AD 50 to AD 1955 (Fig. 2 and Supplementary Fig. S7).

The calculated SOI_{pr} for the past 100 years reveals a multi-decadal variability similar to that seen in the smoothed instrumental SOI time series (Supplementary Fig. S8). Smoothed over 11 years (the averaged resolution of the used palaeo-precipitation record is 11 years), SOI_{pr} and SOI from AD 1867 to AD 1955 have a significant correlation (Supplementary Fig. S8, $r = 0.69$, $p < 0.01$, $n_{eff} = 14.6$). This result is consistent with our analysis above using instrumental rainfall records, confirming that SOI_{pr} is a reliable proxy for the SOI. We also compared our SOI_{pr} with some high resolution ENSO reconstructions over the past 350 years[4,6,7] and found that the multi-decadal variations of SOI_{pr} and these ENSO reconstructions are consistent, but the long term trends are not. For example, the boreal cold-season Niño-3 index, mainly derived from temperature records, showed an obvious trend towards a La Niña-like state over the past 350 years[7], whereas our SOI_{pr}, derived from hydrological records, indicated an opposite trend toward a El Niño-like state. Two other ENSO reconstructions[4,6], based on multiple proxies including temperature records and hydrological records, suggested no obvious trend over the past 350 years.

The reconstructed SOI_{pr} has five distinct centennial-scale phases over the past 2,000 years (Fig. 2): persistent negative values during AD 50–500, AD 1000–1400 and AD 1850–1955, interrupted by positive values during AD 500–1000 and AD 1400–1850. For the past millennium, the SOI_{pr} shows three phases associated with the solar irradiance and background climate state (Fig. 3). Negative SOI_{pr} values (indicating a weak PWC) are associated with higher solar irradiance and global mean temperature during the Medieval Warm Period (MWP) and the so-called Modern Warm Period. On the other hand, positive SOI_{pr} values (indicating an enhanced PWC) are concurrent with lower solar irradiance and cooler global mean temperature during the Little Ice Age (LIA).

The positive SOI_{pr} and enhanced PWC during the relatively cool LIA period (Fig. 2) suggest a more La Niña-like mean state than that during the MWP, contradicting current mainstream theory, mainly from sea surface temperature (SST) reconstruction, about the tropical Pacific ENSO variability or mean state changes over the past millennium (Supplementary Fig. S10). Coral-based SST reconstruction from Palmary Island in the central equatorial Pacific[17] implied a more El Niño-like mean state during the LIA than that in MWP (Supplementary Fig. S10). The SST reconstructions in the western[10,12], eastern[18,19] and mid[17] tropical

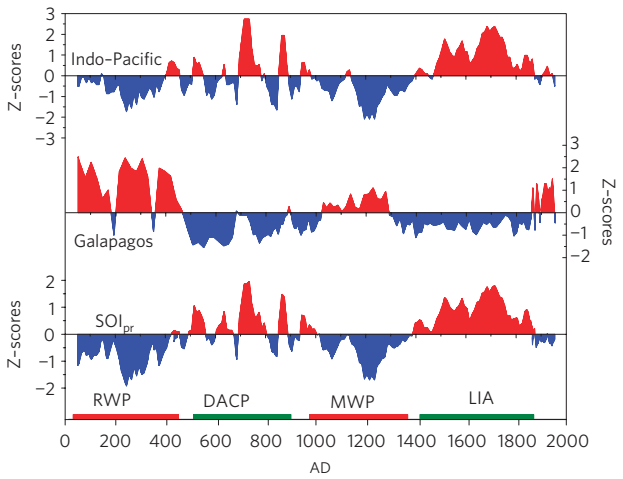

Figure 2 | SOI_{pr} reconstruction. SOI proxy SOI_{pr} as the difference between the reconstructed precipitation records from Indonesia, in the western Pacific (top; ref. 10), and the Galapagos, in the eastern Pacific (middle)[13]. All records were normalized to a standard Z-score before taking the difference (see Methods for detail). High precipitation and positive SOI_{pr} are shown in red and low precipitation and negative SOI_{pr} are shown in blue. Time periods: RWP–Roman Warm Period (AD 50–400), MWP–Medieval Warm Period (AD 1000–1300), DACP–Dark Ages Cold Period (AD 500–900), LIA–Little Ice Age (AD 1400–1850).

Pacific suggested[20,21] an LIA marked by a relatively warming period in the eastern and central tropical Pacific, a substantial cooling in the western equatorial ocean, and a more El Niño-like state (than that of the MWP; Supplementary Fig. S10). In contrast with SST-based reconstructions, most of the hydrological reconstructions from the tropical Pacific suggested a more La Niña-like mean state during the LIA than during the MWP (Fig. 1 and Supplementary Fig. S10). These include records from the Indo-Pacific[8–12], central tropical Pacific[15] and eastern equatorial Pacific[13,14] that suggested wetter, drier and drier conditions, respectively, during the LIA than during the MWP (Fig. 1 and Supplementary Fig. S10). On the other hand, a record of flood deposits near 13° S, on the Peru Margin, indicating wet conditions during the LIA (ref. 22), is also consistent with a more La Niña-like mean state during the LIA. This site experiences dry conditions during El Niño events (Fig. 1 and Supplementary Fig. S2).

Theoretical models and computer simulations also gave contradictory results for the mean state in the LIA and the MWP. The main external forcing difference between the LIA and the MWP is believed to be the minimum solar irradiance (Fig. 3) from about AD 1400 to 1850 (ref. 23) and the near lowest surface temperature in the Northern Hemisphere (NH) and many other places globally over the past millennium[24]. Some models have been proposed for the response of the tropical Pacific ENSO to decreased solar forcing and mean global temperature from the MWP to the LIA. The 'ocean dynamical thermostat' mechanism[25] predicted a more La Niña-like state in the MWP than in the LIA. According to this model, a positive solar forcing and increasing mean global temperature during the MWP would result in a large zonal temperature gradient across the equatorial Pacific. In the western tropical Pacific, rising atmospheric temperature will warm the sea surface, but in the eastern equatorial Pacific, surface warming is restrained owing to the cooling from upwelling. The increased zonal SST gradient enhances the equatorial trade winds, further drives cooling by upwelling, and increases the SST gradient. This model prediction is supported by the SST-based reconstructions[17,20,21] over the past millennium. The most recent coupled general circulation models (CGCM), however, project a weakening of the atmospheric overturning

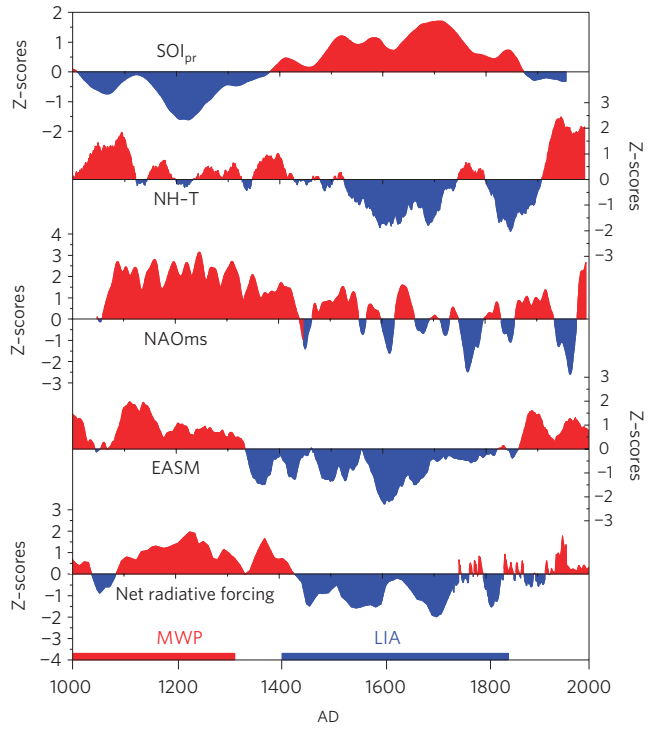

Figure 3 | Linkage between SOI_{pr}, solar irradiance and Northern Hemisphere climate. Comparison of long-term proxy records SOI_{pr}, Northern Hemisphere temperature (NH-T; ref. 24), NAOms (ref. 28), EASM (ref. 29), and solar irradiance[23] over the past millennium. All time series were 30-years smoothed and normalized to a standard Z-score. The correlations among them are presented in Supplementary Table S2.

circulation (especially for the Walker Circulation) as the climate warms, driven by changes in the atmospheric hydrologic cycle[26,27]. The water vapour in the lower troposphere increases by roughly 7% per °C warming[27], whereas precipitation increases more slowly, approximately by 2% per °C warming[27]. The increased moisture has to be transported from the atmospheric boundary layer to the free troposphere, weakening the boundary layer/troposphere mass exchange and tropical overturning circulations[26,27]. This mechanism predicted a less La Niña-like state in the MWP than in the LIA, in agreement with our SOI_{pr} reconstruction and other hydrological records from the tropical Pacific[8–15,22].

The tropical Pacific is important for global climate change[1,3,9], and the interaction between tropical Pacific hydrology and Northern Hemisphere climate is an important aspect of the global climate. In this study, we examined and found a significant link between the reconstructed SOI_{pr} and the Northern Hemisphere temperature for the past millennium (Fig. 3; ref. 24). Negative SOI_{pr}, indicative of a weak PWC, corresponded to the warm climate in the Northern Hemisphere during the Medieval Warm Period and the last century. Positive SOI_{pr} occurred during the relatively cold LIA. The significant correlation ($r = -0.54$, $p < 0.05$, $n_{eff} = 11.94$, AD 1000–1955) suggested a dynamic link between the hydrology in the tropical Pacific and the Northern Hemisphere climate, and this coupling may be established by the interplay between the PWC and the Northern Atlantic Oscillation (NAO; ref. 28), monsoonal circulations[29] and other mechanisms (see Fig. 3 and Supplementary Discussion).

Nonetheless, further research is also needed to reconcile the contradiction between SST and hydrologic reconstructions, to examine whether and how the centennial-scale variations of the Pacific Walker Circulation are related to those of the ENSO during the last millennium, and to study the relationships between the tropical Pacific ENSO and mid-high latitude climate systems over the past millennium and their mechanisms.

Methods

SOI_{pr} calculation. To calculate SOI_{pr}, we first normalized the instrumental and reconstructed precipitation records to the standard Z-score: $Z = (X - V)/SD$; here X is original value; V and SD are the averaged value and standard deviation of the time series. $SOI_{pr} = w_p Z_P - w_n Z_N$; here Z_P and Z_N are the normalized Z-scores of the precipitation in the PA of the western Pacific and in the NA of the eastern and mid Pacific, respectively. w_p and w_n are the optimal weights of Z_P and Z_N and $w_p + w_n = 1$. The values of w_p and w_n are chosen to optimize the correlation between SOI_{pr} and the instrumental SOI (Supplementary Fig. S4).

Error estimation of SOI_{pr}. There are two kinds of uncertainties in the reconstructed SOI_{pr}: non-systematic and systematic. Non-systematic means those errors of local nature, due to dating uncertainties and index measurement errors. For example, the real age of a sample could be either earlier or later than the dated one. The maximum dating uncertainties for the Galapagos record are ±100 years from AD 50 to 1000 and ±60 from AD 1000 to 1890, based on a basal accelerator mass spectrometry (AMS) $AMS^{14}C$ date assessment, and ±5 years in recent 110 years, based on a basal Pb-Cs date assessment[13]. The index measurement errors for the Galapagos record are not available, and we use the mean instrumental error (±1%) instead. The dating uncertainties for the Indonesia record are ±40 years from AD 50 to 1500 ($AMS^{14}C$), ±90 years ($AMS^{14}C$) from AD 1500 to AD 1900, and ±5 years (Pb-Cs) in the last century[10]. The index measurement errors for Indonesia are available. We used Monte Carlo simulations to estimate this kind of uncertainty. In each Monte Carlo simulation, to simulate the index measurement noise, we generated and added Gaussian noise to the proxy records using the available standard deviation and the Box–Muller algorithm[30]. The simulation of dating uncertainties was based on the consideration that the effect of the dating uncertainty is roughly equivalent to temporally shifting the time series by the dating error. For each time point, we calculated the minimum and maximum index values in the window of the dating error and assigned the index value to an evenly distributed random number between the minimum and maximum values. After application of these noises, both records were normalized to the standard Z-score; the difference between the two records was recalculated and denoted as SOI_{pr} (see Methods above). We repeated the Monte Carlo simulation N times, obtained the distribution of $\sim SOI_{pr} - SOI_{pr}$, and calculated the standard deviation for each time point. A Student t test showed no significant differences in the calculated standard deviations between $N = 100$ and $N = 1{,}000$ ($p = 0.69$) and greater, so we chose 1,000 for N. We estimated this uncertainty of SOI_{pr} as two standard deviation (95%) confidence intervals and the result is presented in Supplementary Fig. S7.

The systematic uncertainty arises from the reservoir effect correction, and it affects the dated ages of all subsamples of a time series globally. For example, an over-correction of 10 years will shift all sample ages to be 10 years younger than their actual ages. As SOI_{pr} is the difference between two time series, this kind of uncertainty could have a significant impact. We also used Monte Carlo simulations to estimate this uncertainty. The reservoir age for the Indonesia record is 475 ± 80 years[10], and the estimated reservoir age for the Galapagos record is 0 ± 4 years[13]. In each Monte Carlo simulation, we randomly added from −80 to 80 years and from −4 to 4 years, respectively, to the dated ages for the IPWP and Galapagos records before calculating SOI_{pr}. The other procedures are the same as above. The result of the error estimation from both the systematic uncertainty and the non-systematic uncertainty (combined) is also presented in Supplementary Fig. S7.

Correlation analysis. For two time series, X and Y, the Pearson correlation coefficient r_{xy} was calculated as

$$r_{xy} = \frac{\sum_{i=1}^{n}(x_i - \overline{x})(y_i - \overline{y})}{(n-1)s_x s_y}$$

where n is the number of samples, $\overline{x}$ and $\overline{y}$ are the sample means of X and Y, and S_x and S_y are the sample standard deviation of X and Y.

For two time series (X and Y) with smoothing, we have to consider and adjust the autocorrelation in X and Y by using the effective sample size or effective number of independent values. Following Trenberth (1984; ref 16), and Bretherton *et al.* (1999; ref. 31), we first calculated τ, the time between independent values (or the time to obtain a new degree of freedom) according to the following equation[32]:

$$\tau = 1 + 2\sum_{l=1}^{(n-1)} r_{xl} r_{yl}$$

where r_{xl} and r_{yl} are the autocorrelation at lag l for X and Y. The effective number of independent values was calculated as $n_{eff} = n/\tau$, and the student t-value for assessing significance was calculated as

$$t = \frac{r_{xy}\sqrt{n_{eff} - 2}}{\sqrt{(1 - r_{xy}^2)}}$$

Received 17 May 2011; accepted 13 July 2011; published online 14 August 2011

References

1. Tsonis, A. A., Hunt, A. G. & Elsner, J. B. On the relation between ENSO and global climate change. *Meteorol. Atmos. Phys.* **84,** 229–242 (2003).
2. Trenberth, K. E. & Caron, J. M. The Southern Oscillation revisited: Sea level pressures, surface temperatures, and precipitation. *J. Clim.* **13,** 4358–4365 (2000).
3. Wang, C. Atmospheric circulation cells associated with the El Niño–Southern oscillation. *J. Clim.* **15,** 399–419 (2002).
4. McGregor, S., Timmermann, A. & Timm, O. A unified proxy for ENSO and PDO variability since 1650. *Clim. Past* **6,** 1–17 (2010).
5. Braganza, K., Gergis, J., Power, S., Risbey, J. & Fowler, A. A multiproxy index of the El Nino–Southern Oscillation, AD 1525–1982. *J. Geophys. Res.* **114,** D05106 (2009).
6. Stahle, D. *et al.* Experimental dendroclimatic reconstruction of the Southern Oscillation. *Bull. Am. Meteorol. Soc.* **79,** 2137–2151 (1998).
7. Mann, M. *et al.* Global temperature patterns in past centuries: An interactive presentation. *Earth Interact.* **4,** 1–1 (2000).
8. Yan, H. *et al.* South China Sea hydrological changes and Pacific Walker Circulation variations over the last millennium. *Nature Commun.* **2,** 293 (2011).
9. Tierney, J., Oppo, D., Rosenthal, Y., Russell, J. & Linsley, B. Coordinated hydrological regimes in the Indo-Pacific region during the past two millennia. *Paleoceanography* **25,** PA1102 (2010).
10. Oppo, D. W., Rosenthal, Y. & Linsley, B. K. 2,000-year-long temperature and hydrology reconstructions from the Indo-Pacific warm pool. *Nature* **460,** 1113–1116 (2009).
11. Liu, X. D. *et al.* A 1,100-year palaeoenvironmental record inferred from stable isotope and trace element compositions of ostracode and plant caryopses in sediments of Cattle Pond, Dongdao Island, South China Sea. *J. Paleolimnol.* **40,** 987–1002 (2008).
12. Newton, A., Thunell, R. & Stott, L. Climate and hydrographic variability in the Indo-Pacific Warm Pool during the last millennium. *Geophys. Res. Lett.* **33,** L19710 (2006).
13. Conroy, J. L., Overpeck, J. T., Cole, J. E., Shanahan, T. M. & Steinitz-Kannan, M. Holocene changes in eastern tropical Pacific climate inferred from a Galapagos lake sediment record. *Quat. Sci. Rev.* **27,** 1166–1180 (2008).
14. Moy, C. M., Seltzer, G. O., Rodbell, D. T. & Anderson, D. M. Variability of El Nino/Southern Oscillation activity at millennial timescales during the Holocene epoch. *Nature* **420,** 162–165 (2002).
15. Sachs, J. P. *et al.* Southward movement of the Pacific intertropical convergence zone AD 1400–1850. *Nature Geosci.* **2,** 519–525 (2009).
16. Trenberth, K. Signal versus noise in the Southern Oscillation. *Mon. Weather Rev.* **112,** 326–332 (1984).
17. Cobb, K. M., Charles, C. D., Cheng, H. & Edwards, R. L. El Nino/Southern Oscillation and tropical Pacific climate during the last millennium. *Nature* **424,** 271–276 (2003).
18. Conroy, J. L. *et al.* Unprecedented recent warming of surface temperatures in the eastern tropical Pacific Ocean. *Nature Geosci.* **2,** 46–50 (2009).
19. Kennett, D. J. & Kennett, J. P. Competitive and cooperative responses to climatic instability in coastal southern California. *Am. Antiquity* **65,** 379–395 (2000).
20. Conroy, J. L., Overpeck, J. T. & Cole, J. E. El Nino/Southern Oscillation and changes in the zonal gradient of tropical Pacific sea surface temperature over the last 1.2 ka. *PAGES News* **18,** 32–34 (2010).
21. Graham, N. E. *et al.* Tropical Pacific—mid-latitude teleconnections in medieval times. *Clim. Change* **83,** 241–285 (2007).
22. Rein, B. *et al.* El Nino variability off Peru during the last 20,000 years. *Paleoceanography* **20,** PA4003 (2005).
23. Bard, E., Yiou, Raisbeck & Jouzel, G. Solar irradiance during the last 1200 years based on cosmogenic nuclides. *Tellus* **52,** 985–992 (2000).
24. Mann, M. *et al.* Proxy-based reconstructions of hemispheric and global surface temperature variations over the past two millennia. *Proc. Natl Acad. Sci.* **105,** 13252 (2008).
25. Mann, M., Cane, M., Zebiak, S. & Clement, A. Volcanic and solar forcing of the tropical Pacific over the past 1000 years. *J. Clim.* **18,** 447–456 (2005).
26. Vecchi, G. A. *et al.* Weakening of tropical Pacific atmospheric circulation due to anthropogenic forcing. *Nature* **441,** 73–76 (2006).
27. Held, I. & Soden, B. Robust responses of the hydrological cycle to global warming. *J. Clim.* **19,** 5686–5699 (2006).
28. Trouet, V. *et al.* Persistent positive north atlantic oscillation mode dominated the medieval climate anomaly. *Science* **324,** 78–80 (2009).
29. Zhang, P. Z. *et al.* A test of climate, sun, and culture relationships from an 1810-Year Chinese cave record. *Science* **322,** 940–942 (2008).
30. Box, G. E. P & Muller, M. E. A note on the generation of random normal deviates. *Ann. Math. Stat.* **29,** 610–611 (1958).
31. Bretherton, C. S., Widmann, M., Dymnikov, V. P., Wallace, J. M. & Blade, I. The effective number of spatial degrees of freedom of a time-varying field. *J. Clim.* **12,** 1990–2009 (1999).
32. Box, G. E. P., Jenkins, G. M. & Reinsel, G. C. *Time Series Analysis: Forecasting and Control* Vol. 16 (Holden-Day San Francisco, 1976).

Acknowledgements

Financial support for this research was provided by the Natural Science Foundation of China (NSFC) (40730107) and the Major State Basic Research Development Program of China (973 Program) (No.2010CB428902).

Author contributions

H.Y., L.S. and Y.W. designed the study and wrote the paper; Y.W., W.H., S.Q. and C.Y. contributed to the statistical analysis and improving the English; all authors discussed the results and implications and commented on the manuscript at all stages.

Additional information

The authors declare no competing financial interests. Supplementary information accompanies this paper on www.nature.com/naturegeoscience. Reprints and permissions information is available online at http://www.nature.com/reprints. Correspondence and requests for materials should be addressed to L.S.